Microchimica Acta (2019) 186: 169
https://doi.org/10.1007/s00604-019-3282-3

ORIGINAL PAPER

An impedimetric biosensor for *E. coli* O157:H7 based on the use of self-assembled gold nanoparticles and protein G

Donghai Lin[1,2] · Rajesh G. Pillai[3] · William Edward Lee[4,5] · Abebaw B. Jemere[3]

Received: 6 November 2018 / Accepted: 23 January 2019 / Published online: 11 February 2019

Abstract

Two kinds of electrochemical impedimetric biosensors for the detection of *E. coli* O157:H7 are described and compared. They were fabricated using self-assembled layers of thiolated protein G (PrG-thiol) on (i) planar gold electrodes and (ii) gold nanoparticles (Au NPs) modified gold electrodes. The fabrications of the biosensors were characterized using cyclic voltammetry, electrochemical impedance spectroscopy, scanning electron microscopy and atomic force microscopy techniques. The modification of the planar gold electrode by Au NPs via self-assembled monolayer of 1,6-hexadithiol as a linker molecule increased the electrochemically active surface area by about 2.2 times. The concentration of PrG-thiol and its incubation time, as well as the concentration of IgG were optimized. The Au NP-based biosensor exhibited a limit of detection of 48 colony forming unit (cfu mL^{-1}) which is 3 times lower than that of the planar gold electrode biosensor (140 cfu mL^{-1}). It also showed a wider dynamic range (up to 10^7 cfu mL^{-1}) and sensitivity. The improved analytical performance of the Au NP-modified biosensor is ascribed to the synergistic effect between the Au NPs and the PrG-thiol scaffold. The biosensor exhibited high selectivity for *E. coli* O157:H7 over other bacteria such as *Staphylococcus aureus* and *Salmonella typhimurium*.

Keywords Electrochemical impedance spectroscopy · Gold nanoparticles · Oriented antibody immobilization · E. Coli · Pathogen detection · Biosensor

Electronic supplementary material The online version of this article (https://doi.org/10.1007/s00604-019-3282-3) contains supplementary material, which is available to authorized users.

✉ Abebaw B. Jemere
abebaw.jemere@nrc-cnrc.gc.ca

William Edward Lee
platinum@telusplanet.net

[1] Department of Chemistry, University of Alberta, Edmonton, AB T6G 2G2, Canada

[2] Present address: School of Food Science and Engineering, Foshan University, Foshan, China

[3] National Research Council Canada – Nanotechnology Research Centre (Formerly known as National Institute for Nanotechnology), 11421 Saskatchewan Drive, Edmonton, AB T6G 2M9, Canada

[4] Defence Research and Development Canada – Suffield Research Centre, Medicine Hat, AB T1A 8K6, Canada

[5] Present address: Platinum Research and Technologies, Medicine Hat, Alberta, Canada

Introduction

Rapid, sensitive and selective detection of pathogens is pivotal to secure food safety and protect public health. *Escherichia coli* O157:H7 (*E. coli* O157:H7) is one of the most dangerous pathogens infecting millions of people worldwide [1], primarily caused by consumption of contaminated food products. With an infectious dose as low as 10 bacterial cells [2, 3], infection of *E. coli* O157:H7 typically causes bloody diarrhea, which may lead to hemolytic-uremic syndrome [4]. Consuming *E. coli* O157:H7 contaminated food not only menaces human health but also can cause huge economic loss [5]. Thus, rapid methods of *E. coli* O157:H7 detection in food products are needed.

The common methods of pathogenic bacteria detection, such as colony counting, PCR and ELISA are slow, labor intensive, expensive and are not amenable for on-site use [6]. Biosensors are attractive alternatives due to their simplicity, sensitivity, low cost, speed and applicability for real-time

on-site measurement of pathogenic bacteria [7, 8]. Several biosensors for the detection of *E. coli* based on the specific interaction between antibodies and antigens using optical [9], mass [10] and electrochemical [11] signal transduction methods have been reported. Among electrochemical biosensors, electrochemical impedance spectroscopy (EIS)-based detection of pathogens is attractive due to its non-destructive and label-free nature, simplicity of operation, amenability to miniaturization and the low detection limits it can achieve [12, 13]. The forte of the technique is its ability to measure subtle changes in electrical properties of an electrode surface in response to changes in the material composition of the surface, in particular, changes arising from receptor-ligand interactions.

In EIS biosensors fabrication, modification of electrode surfaces with nanomaterials to enhance the electrode properties has received considerable attention [14–16]. Gold nanoparticles (Au NPs) are one of the most promising nanomaterials that opened new prospects in the fabrication of EIS biosensors due to their unique electrical properties, ease of preparations, good biocompatibility, and the large surface area-to-volume ratio they can provide [17–20]. Wang et al. [21] electrodeposited gold nanoparticles onto a graphene oxide-modified paper electrode for physisorption of a polyclonal antibody and reported a limit of detection (LOD) of 150 colony forming units mL (cfu mL^{-1}) for *E. coli* O157:H7. This value is similar to other reported LODs (10^2–10^3 cfu mL^{-1}) for EIS detection of *E. coli* O157:H7 using planar electrodes [22–24]. However, the high virulence nature and a low infective dose of *E. coli* O157:H7 [2, 3] call for the development of sensors with lower limits of detection. To the best of our knowledge, only three research groups have reported on EIS-based *E. coli* O157:H7 sensors with LOD of 10 or less cfu mL^{-1}. Maalouf et al. [25] reported an impedimetric *E. coli* sensor with a LOD of 10 cfu mL^{-1} using biotinylated antibody tethered to a neutravidin self-assembled monolayer (SAM) on a planar gold surface. Dos Santos et al. [26, 27] reported LOD of 1–2 cfu mL^{-1} using *E.coli* antibody tethered to 11-mercaptoundecanoic acid SAM on planar gold electrode and methoxysilane modified planar ITO electrode. Joung et al. [28] also reported a LOD of 10 cfu mL^{-1} for *E. coli* O157:H7 using a methoxysilane modified alumina nanoporous membrane for antibody immobilization. Silanizing the electrode surfaces for antibody immobilization means the sensors are single use disposable, which may not be ideal for self-contained integrated modular electrochemical sensors. In this work, we report the fabrication and characterization of a sensitive, selective and reusable label-free impedimetric sensor for heat-killed *E. coli* O157:H7 (HKEC) using oriented antibody immobilization strategy and gold nanoparticles, achieving LOD of 48 cfu mL^{-1}.

For oriented immobilization of antibody, we used thiolated protein G (PrG-thiol) that self-assembles on gold surfaces as an intermediary layer. Antibody binding proteins such as PrG are commonly used to immobilize antibodies on solid supports [29–33] and have the ability to bind non-antigenic (Fc) portions of immunoglobulin G (IgG), leaving the antigen-binding (Fab) fragments well aligned with minimal steric hindrance. Well-oriented surface immobilized antibodies can increase antigen-binding capacity by about 2–8 times [34], which would lower the detection limit, and increase the sensitivity and dynamic range of a biosensor [35]. Herein, two methods were examined to immobilize PrG on the surface of the sensor electrodes. Method one used direct attachment of a recombinant thiolated PrG to the Au electrode surface and method two involved an intermediary layer of Au NPs to attach the PrG-thiol. The intent was to compare the performance of the EIS sensor with and without the Au NP layer.

We reported an electrochemical reductive desorption technique to repeatedly desorb and self-assemble an Au NP-loaded SAM sensor surface for electrochemical impedance spectroscopy (EIS) detection of viruses and oligonucleotides [18, 36]. We employed a similar strategy here and developed a sensitive, regenerable EIS biosensor for detection of HKEC. The overall reproducibility of the sensor layers was high, the relative standard deviation (%RSD) was <1% for sensor fabrication (i.e. antibody modified electrodes) ($n = 5$) and <12% for calibration results ($n = 3$). The presence of Au NP layer on the sensor surface increased the sensitivity of the sensor, primarily at the low concentration regime and provided lower limits of detection (48 cfu mL^{-1}) than the sensor fabricated on planar gold electrodes (140 cfu mL^{-1}).

Experimental part

Chemicals and materials

1,6-Hexanedithiol (1,6-HDT), phosphate buffered saline (PBS) tablets, $K_4[Fe(CN)_6]$, $K_3[Fe(CN)_6]$, KNO_3, gold nanoparticles (dia. 10 nm, 6×10^{12} particles mL^{-1} in 0.1 mM PBS) and bovine serum albumin (BSA) were purchased from Sigma-Aldrich Canada (Canada, www.sigmaaldrich.com). Anhydrous ethyl alcohol was obtained from Commercial Alcohols Inc. (Canada, www.comalc.com). Recombinant protein G-thiol (PrG-thiol) was obtained from Protein Mods (USA, www.proteinmods.com). Heat-killed *Staphylococcus aureus* (HKSA) and heat-killed *salmonella typhimurium* (HKST) were obtained from Cedarlane (Canada, www.cedarlanelanbs.com). Affinity purified goat anti-*E. coli* O157:H7 IgG and heat-killed *E. coli* O157:H7 (HKEC) (3×10^9 cfu mL^{-1}) were purchased from SeraCare Life Sciences (USA, www.seracare.com). Pierce™ protein G IgG-binding buffer, pH 5.0, was purchased from ThermoFisher Scientific (Canada, www.fishersci.ca). Deionized water having a resistivity of 18 MΩ.cm (Milli-Q UV Plus Ultra-Pure

Millipore System) was used for aqueous solutions preparation and rinsing electrodes. Phosphate buffered saline (PBS) tablets were dissolved in deionized water to make a 10 mM pH 7.4 buffer.

Biosensor preparation

Scheme 1 shows the stepwise fabrication of the biosensors. First, Au electrodes with a diameter of 6 mm (area equals 0.28 cm^2) were fabricated on glass slide substrates (2.5 × 7.5 × 0.1 cm) at the University of Alberta NanoFab (Edmonton, AB) as described before [18]. In the preparation of planar gold electrode-based biosensor (Scheme 1a), 200 μL aliquot of freshly prepared PrG-thiol in PBS was applied to the electrode surface in a humidified environment for varying times at room temperature. After rinsing with copious amounts of PBS solution, the electrode was incubated with varying concentrations of 200 μL anti-*E. coli* IgG (prepared in binding buffer) for 2 h at room temperature to produce the biosensor. The sensor was then washed with the binding buffer and incubated with 200 μL of 1 mg mL^{-1} BSA in PBS for 30 min to block non-specific binding sites. Following washing with PBS, the biosensor was incubated with an aliquot of 200 μL of HKEC in PBS for 2 h. Electrodes were thoroughly rinsed with water and dried in a N_2 stream before electrochemical measurements.

In the preparation of Au NP-modified electrode (Scheme 1b), the gold electrode was first incubated with 10 mM ethanolic solution of 1,6-HDT for 12 h. The modified electrode (Au/1,6-HDT) was then rinsed with ethanol followed by water and dried with N_2 prior to incubation with 200 μL of Au NPs (1.2×10^{12} particles) for 2 h to obtain the Au NP modified electrode surface (Au/1,6-HDT/AuNP). The Au/1,6-HDT/AuNP electrode was then rinsed with water and incubated with 500 μg mL^{-1} PrG-thiol in PBS for 8 h. The Au/1,6-HDT/AuNP/PrG electrode was rinsed with PBS and treated with 200 μL of 10 μg mL^{-1} anti-*E. coli* O157:H7 IgG for 2 h to produce the complete biosensor surface. The sensor was then washed with the binding buffer and incubated with 200 μL of 1 mg mL^{-1} BSA in phosphate buffered saline for 30 min to block non-specific binding sites. Lastly, the biosensor was incubated with 200 μL of the antigen (HKEC in PBS) for 2 h. Electrodes were thoroughly rinsed with water and dried with N_2 before electrochemical measurements.

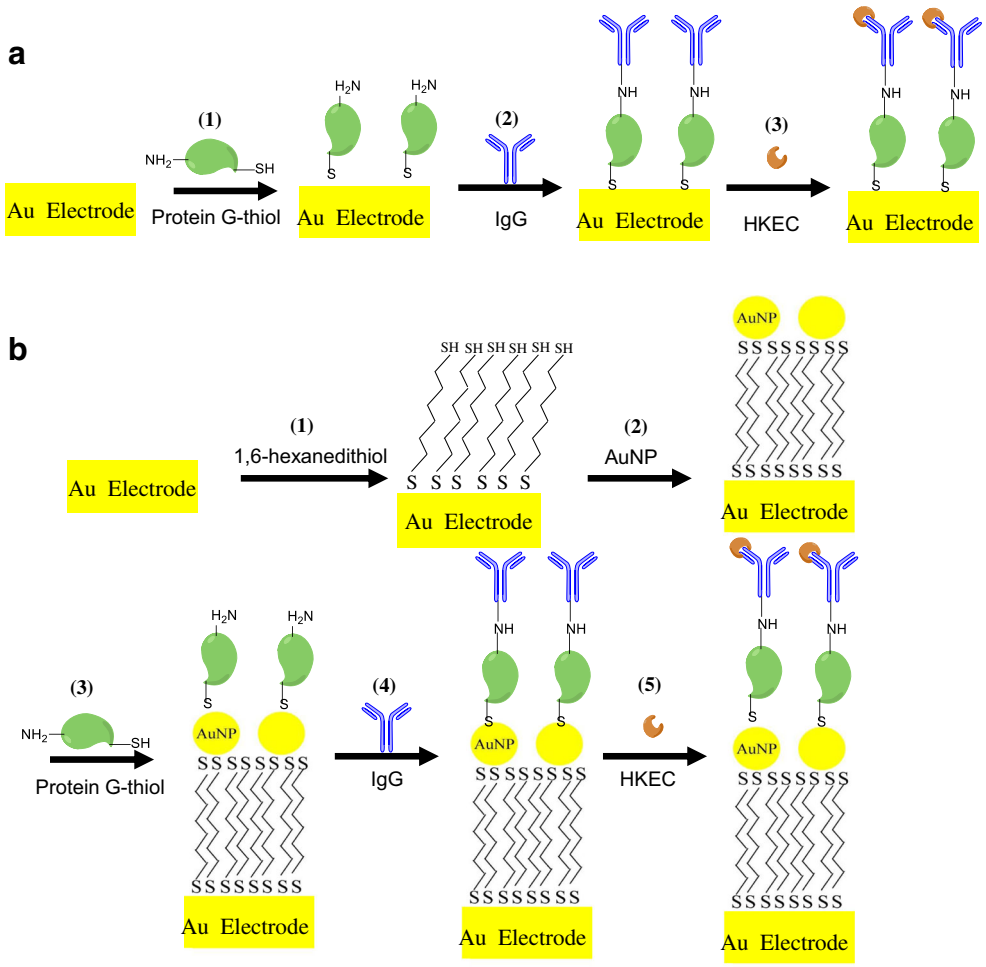

Scheme 1 Schematic representations of sensor fabrication using (**a**) planar Au electrode and (**b**) Au NP-modified electrode (HKEC = heat killed *E. coli* O157:H7)

The sensor fabrication steps were characterized by Hitachi S-4800 scanning electron microscopy (SEM), Dimension 3100 atomic force microscopy (AFM, Digital Instruments, Buffalo, NY), cyclic voltammetry (CV) and EIS. Image J software (National Institute of Health) was used to calculate the number of gold nanoparticles from the SEM image.

Electrochemical measurements and biosensor surface regeneration

Electrochemical measurements were performed at room temperature with a Gamry Reference 600™ Potentiostat (USA, www.gamry.com) and a three-electrode system that consisted of a modified Au electrodes (described above) as the working electrode, a Pt wire as a counter electrode and Ag/AgCl reference electrode from BASi (USA, www.basinc.com). The redox probe was 1 mM $K_4[Fe(CN)_6]/K_3[Fe(CN)_6]$ in 0.1 M KNO_3 solution. All CV studies were performed at −0.2 V to +0.7 V vs. Ag/AgCl at a scan rate of 100 mV s^{-1}. Impedance measurements were made with a 10 mV sinusoid superimposed on a DC potential of +0.21 V vs. Ag/AgCl with a frequency range of 0.1 Hz to 100 kHz. A Randles equivalent circuit and a Gamry-supplied software were used to obtain the values of circuit components. The change in charge transfer resistance on the sensor's surface was used to make calibration plots for both specific receptor-ligand binding and non-specific binding. Electrochemical reductive desorption, by applying a potential of −1.2 V to the modified gold electrode vs. Ag/AgCl for a total of 3 min, was used to regenerate the working gold electrode as described before [18, 36]. Regenerated Au surfaces were characterized by CV and EIS.

Results and discussion

Fabrication and characterization of electrochemical sensors

Effects of protein G concentration and incubation time on planar gold electrode

Figure 1a shows the CV of $Fe(CN)_6^{3-/4-}$ as a function of the concentration of PrG-thiol incubated for 1 h. The bare Au electrode (PrG concentration = 0 μg mL^{-1}) showed a quasi-reversible redox behavior with a peak-to-peak separation potential (ΔEp) of ~0.11 V. As the concentration of PrG-thiol in the incubation solution was increased (0–1000 μg mL^{-1}), the redox current decreased, showing negligible change in peak current after 500 μg mL^{-1} of PrG-thiol. These results indicated maximum adsorption of PrG-thiol on the electrode and increased passivation of the electrode through the formation of the PrG-thiol SAM.

The corresponding impedance responses (Nyquist plots) after SAM formation with different concentrations of PrG-thiol are shown in Fig. 1b. As can be seen, the Nyquist plots consist of two portions. The semicircle portion at high frequencies indicates the electron-transfer process through the SAM while the linear part at lower frequencies represents the diffusion-limited mass transfer process of the redox probe. The inset in Fig. 1b shows the Randles equivalent circuit to which the impedance data were fitted to determine the experimental values of the circuit elements (See Supplemental Table S1). The circuit elements are described in the caption of Fig. 1. The quality of the data fit to the equivalent circuit was evaluated by an acceptance error value ($\chi^2 < 0.001$). The charge transfer resistance (R_{ct}) of the bare Au electrode was 174 Ω. The values of R_{ct} associated with the Nyquist plots are given in Fig. 1c and are seen to increase from 185 Ω for 10 μg mL^{-1} PrG-thiol solution to a near maximum of approximately 3500 Ω for incubation with 1000 μg mL^{-1} PrG-thiol. The reason for the rise in R_{ct} is that the PrG-thiol forms an insulating SAM on the electrode surface, blocking the electron transfer of $Fe(CN)_6^{3-/4-}$. Similar to the CVs shown in Fig. 1a, when the concentration of PrG-thiol was over 500 μg/ml, the R_{ct} reached a plateau, indicating maximum adsorption of PrG-thiol on the electrode and thus 500 μg mL^{-1} PrG-thiol was selected to make the sensor.

One of the pivotal factors in the assembly of thiolic monolayers is the incubation time [37]. The formation of the PrG-thiol SAM on gold electrode was studied by EIS and CV as a function of incubation time (1 h – 12 h) using a fixed concentration (500 μg mL^{-1}) of PrG-thiol. It is reasonable to assume that highly compact monolayers are practically insulating under usual electrochemical conditions, except when pinholes exist due to structural imperfections. Pinholes allow molecules and ions, from the electrolyte solutions, to reach the electrode. Both the CV and Nyquist plots depicted in Supplementary Fig. S1 show that the redox activity of $Fe(CN)_6^{3-/4-}$ is inhibited as the monolayer becomes more compacted with time, reaching a constant after 8 h of incubation (Fig. 2). Therefore, an incubation time of 8 h for PrG-thiol was used in subsequent experiments. From the change in charge transfer resistance shown in Fig. 2, we calculated the fractional surface coverage (Θ) of the electrode by the PrG-thiol SAM after the optimal 8 h of incubation using Eq. 1

$$\Theta = 1 - \left(R_{ct}^{bare} / R_{ct}^{SAM}\right) \quad (1)$$

where R_{ct}^{bare} is the charge transfer resistance of the clean bare electrode (174 Ω), and R_{ct}^{SAM} is the charge transfer resistance after incubation in PrG-thiol solution [38]. The surface coverage was found to be 98.8%. The mole amount of PrG-thiol self-assembled onto the gold electrode (Γ) also was calculated by integrating the charge (Q) associated with

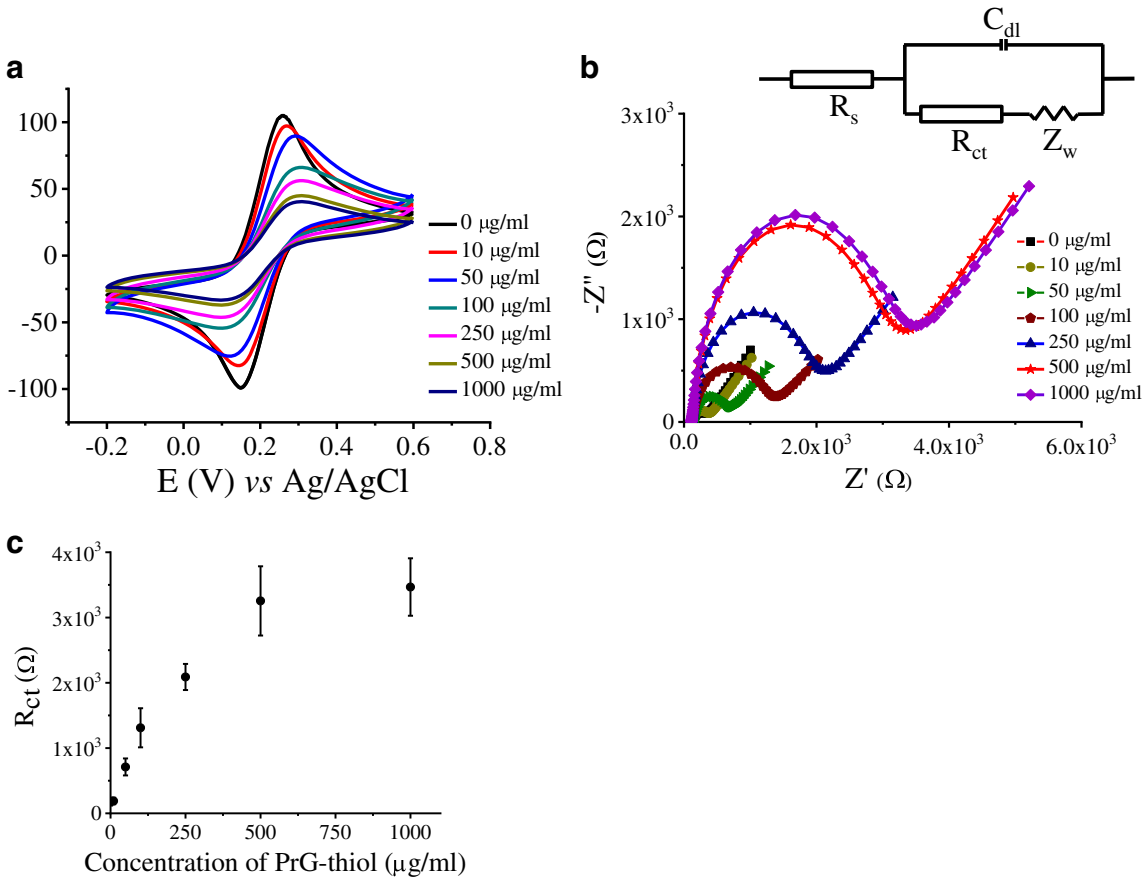

Fig. 1 **a** Cyclic voltammograms of different concentration of PrG-thiol modified planar gold electrodes (1 h incubation) at a scan rate of 100 mV s^{-1} in 1 mM $K_4[Fe(CN)_6/K_3[Fe(CN)_6]$ containing 0.1 M KNO_3 supporting electrolyte using Ag/AgCl as reference electrode and Pt wire as counter electrode. **b** Nyquist plots of PrG-thiol modified planar gold electrodes. The frequency for the impedance measurements was varied from 0.1 Hz to 100 kHz. All other experimental parameters are as in (**a**). The inset shows the Randles equivalent circuit used for all fits. R_s is the solution resistance; C_{dl} is the electrode double layer capacitance; Z_w is the Warburg impedance and R_{ct} is the charge transfer resistance at the electrode surface. **c** Plot of charge transfer resistance (R_{ct}) extracted from the data in (**b**) using the Randles equivalent circuit as a function of PrG-thiol concentration ($n = 3$)

the reductive desorption peak at −0.95 V shown in Supplementary Fig. S2 using Eq. 2

$$\Gamma = Q/nFA \quad (2)$$

where n is the number of electrons involved in the electrode reaction, F is Faraday constant and A is the geometrical area of the electrode. Similar to the report by Fowler et al. [29], the shape of the PrG-thiol desorption voltammograms showed two peaks. Fowler et al. [29] attributed the more negative peak to the reduction of the Au-S bond at stepped Au sites or to desorption at more densely packed protein region. The value of Γ obtained using Eq. 2 was 32 pmol mm^{-2}, which is similar to what Fowler et al. [29] reported (41 pmol mm^{-2}) for PrG-thiol immobilized on a gold electrode.

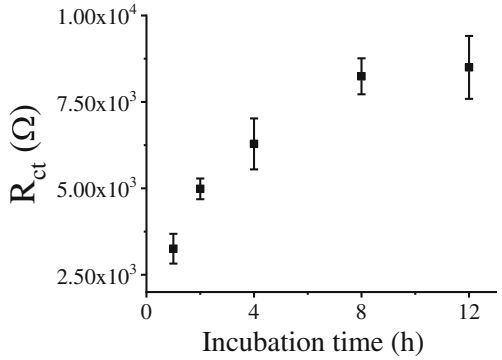

Fig. 2 Plot of R_{ct} versus incubation time ($n = 3$)

Immobilization of immunoglobulin G on protein-G SAM

Biosensor surfaces were fabricated according to Scheme 1a step 2 by incubating PrG-thiol SAM with anti-*E. coli* IgG. The effect of the concentration of IgG on immobilization was studied for a fixed 2 h of incubation with the PrG-thiol modified electrode. The CV curves shown in Fig. 3a show a significant decrease in current with increasing IgG concentration. The maximum passivation resulting from the formation of this second monolayer occurred after 10 µg mL^{-1} of IgG,

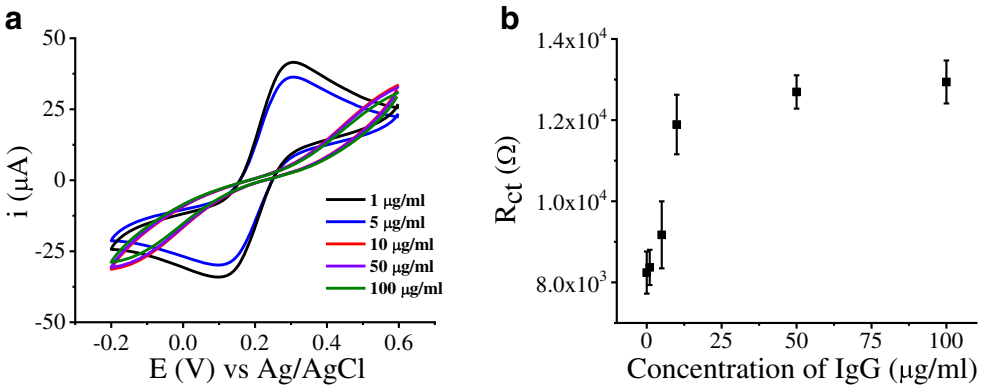

Fig. 3 **a** Cyclic voltammograms of Au/PrG electrode modified with different concentration of anti-*E.coli* IgG at a scan rate of 100 mV s^{-1}, **b** Plot of change in charge transfer resistance (ΔR_{ct}) as a function of the concentration of IgG ($n = 3$)

decreasing the anodic current at 0.3 V from about 40 μA at 1 μg mL^{-1} IgG to about 3 μA at 10 μg mL^{-1} IgG. The R_{ct} values (Fig. 3b) extracted from the Nyquist plots shown in Supplementary Fig. S3 also show addition of IgG to the PrG-thiol SAM produced a concentration-dependent increase in the R_{ct} of the PrG-thiol modified surface, reaching a plateau at 10 μg mL^{-1} IgG concentration. Thus, 10 μg mL^{-1} of IgG was used in the fabrication of the biosensor.

Detection of heat-killed E. coli O157:H7 (HKEC) on planar gold electrode-based electrochemical sensor

Under optimal conditions, the biosensor was tested using HKEC in PBS. The resulting electrochemical changes were monitored by CV and EIS. Supplementary Fig. S4a shows the CV response for each step in the sensor fabrication, Scheme 1a. Addition of HKEC (1×10^5 cfu mL^{-1}, 1 h incubation) to the biosensor did not affect the CV response. The surface already was highly passivated by the previous step of formation of the IgG layer, thus formation of an adsorbed layer of HKEC on the sensor surface left the voltammogram mostly unchanged. In the EIS experiment of the same sample (1×10^5 cfu mL^{-1}, 1 h incubation), the change in R_{ct} was significant (Fig. S4b), approximately 8.5 kΩ, about 65% increase. The Nyquist plots for each step in the sensor fabrication are given in Supplementary Fig. S4b and the circuit elements are shown in Supplementary Table 1.

Nyquist plots of the biosensor response to the range of concentrations (10^0–2.5×10^8 cfu mL^{-1}) are given in Fig. 4a. The diameters of the semicircles in the Nyquist plots expanded upon incubation with increasing concentration, indicating that a greater amount of analyte material was bound to the sensor which in turn generated increased R_{ct}, i.e., increased inhibition of electron transfer of the redox probe. The values of ΔR_{ct} associated with the Nyquist plots, where $\Delta R_{ct} = R_{ct}$ (IgG + HKEC) – R_{ct} (IgG), are plotted as a dose-response in Fig. 4b (solid square). The plot reached a plateau above 10^7 cfu mL^{-1} of HKEC. Each data point represented a mean value obtained from three independent sensors fabricated on the same manifold and tested in parallel; error bars were the standard deviation (sd) of the three measurements. The theoretical limit of detection of the sensor, calculated as 3 × sd/slope, where slope was determined from a linear plot in the concentration range of 10^0 - 10^3 cfu mL^{-1} ($Y = 194.6 + 0.6897$[HKEC], $R^2 = 0.9984$) was calculated to be 140 cfu mL^{-1}. This value is an order of magnitude lower than or comparable to literature reported label-free electrochemical *E. coli* sensors using planar electrodes [22–24]. The % relative standard deviation (%RSD) of R_{ct} for the sensor (R_{ct} (Ig)) measured in buffer was 0.6% ($n = 5$), indicating the high reproducibility of the sensor's fabrication.

Detection of heat-killed E. coli O157:H7 (HKEC) on a gold nanoparticle-mediated electrochemical sensor

An electrochemical sensor incorporating Au NP was fabricated as depicted by Scheme 1b and its performance was compared with that of the planar gold electrode sensor described above. The CV and EIS data following each step of the Au NP-mediated sensor fabrication are depicted in Supplementary Fig. S5. In this fabrication process, the gold electrode was first covered with a SAM of 1,6-hexanedithiol (1,6-HDT), which caused drastic shape change in the CV indicating that HDT formed a well-packed passivation layer on the electrode surface. After self-assembly of Au NPs on the 1,6-HDT modified gold electrode, the CV and EIS data were similar to that of the bare gold electrode, suggesting that the Au NPs rendered a path to promote the transfer of electrons between $Fe(CN)_6^{3-/4-}$ and the electrode as has been previously reported for Au NP-mediated surfaces [18, 36, 39].

Figure 5 shows the AFM and SEM images of Au NP-modified gold electrodes. The surface roughness and height of the modified electrode are shown in Supplementary Fig. S6. These images show that the Au NPs have been embedded onto the 1,6-HDT modified gold electrode surface, and from the SEM image shown in Fig. 5a (using ImageJ software) we estimated the surface coverage of Au NPs to be 1.7×10^{10} particles cm^{-2}. The electroactive surface areas of an Au NP-

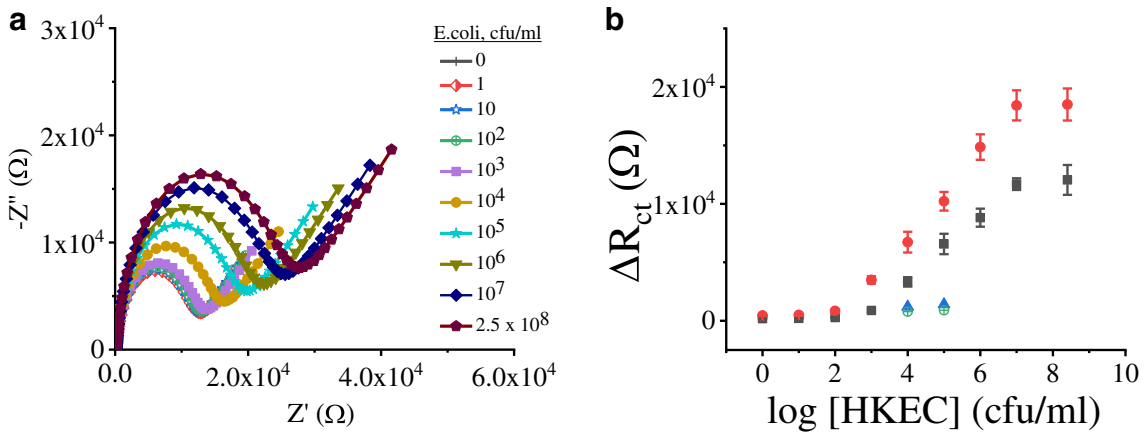

Fig. 4 **a** Nyquist plots of the Au/PrG/Ab sensor after 2 h of incubation with different concentrations of HKEC. **b** Calibration plot of ΔR_{ct} of the planar Au/PrG/Ab (square) and Au NP-modified Au/1,6-HDT/PrG/Ab (circle) electrodes, vs. the logarithm of concentration ($n = 3$). Also shown are the two negative controls, heat-killed *S. aureus* (open circle) and heat-killed *S. thyphimurium* (solid triangle) at concentrations indicated ($n = 3$). All experimental conditions are as in Figs. 1 and 2

modified electrode and a bare gold electrode were measured by CV in 0.5 M H_2SO_4 (Supplementary Fig. S7). Modification of the planar gold electrode by 1,6-HDT significantly reduced the electroactive area of the planar gold electrode, as indicated by the sharp reduction in current density. Following incubation with Au NPs, the current density of the surface was significantly increased since the Au NPs are electroactive. Assuming a specific charge of 400 μC cm^{-2} is required for polycrystalline gold oxidation [40], the electroactive surface area of the Au NP-modified electrode was calculated to be about 2.2 times that of the planar gold electrode, which is similar to a literature reported value [41]. Improvement in electrochemical signal, and by extension, in the electroactive surface area is rationalized by the well-documented large surface area-to-volume ratio provided by Au NPs compared to planar Au electrode [17].

Stepwise construction of PrG-thiol and IgG monolayers onto the Au NPs containing surface (Scheme 1b, steps 3 and 4) resulted in increased R_{ct}. From the EIS response of the Au NP-mediated sensor to HKEC (10^0–2.5×10^8 cfu mL^{-1}), data not shown, typical semicircle responses were recorded, and the diameter of the semicircle increased with the concentration of HKEC added. The values of ΔR_{ct} associated with Nyquist plots, where $\Delta R_{ct} = R_{ct}$ (HKEC+IgG) – R_{ct}(IgG), are plotted as a dose response curve in Fig. 4b (solid circle). Each data point represented an average of three independent measurements, with error bars showing the standard deviation (sd) of the three measurements. The LOD for the Au NP-mediated sensor, calculated as 3 × sd/slope was found to be 48 cfu mL^{-1}. (Slope was determined from a linear plot in the concentration range of 10^0–10^3 Cfu mL^{-1}; $Y = 453.2 + 3.112$[HKEC], $R^2 = 0.9932$) This value is within clinically relevant range and is similar to the lowest LOD reported for EIS detection of *E. coli* O157:H7 [25–28] and 3–10 times lower than what was achieved using planar gold electrode described above, and to most literature reported *E. coli* O157:H7 EIS biosensors [21–24]. The value is also 3 orders of magnitude lower than reported values for surface plasmon resonance-based *E. coli* O157:H7 sensors [25, 42]. The low LOD reported here might be due to the robust immobilization

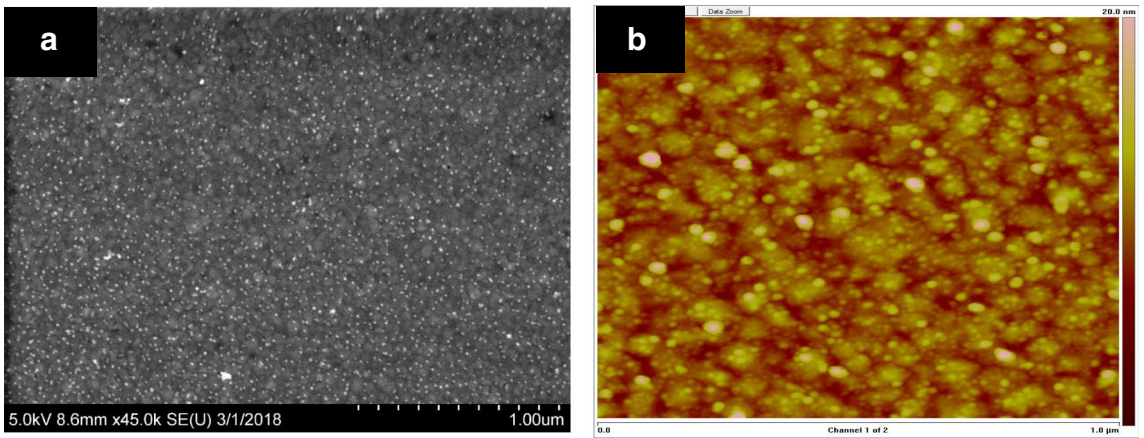

Fig. 5 SEM (**a**) and AFM (**b**) images of gold nanoparticles modified electrode (Au/1,6-HDT/AuNP)

protocol used and the use of gold nanoparticles that increase the surface area of the electrode. An oriented IgG immobilization using protein G as a linker molecule is shown to reduce a LOD by 100 fold [35]. From the slopes of the lines in Fig. 4b, we also estimated the sensitivity of the Au NP-modified electrode to be 1.3 times higher than that of planar gold electrodes in the concentration ranges of 10^3–10^7 cfu mL^{-1} and 4.5 times higher in the lower concentration ranges (10^0–10^3 cfu mL^{-1}), which is consistent with the observed decrease in limit of detection for Au NP-modified electrode based biosensor. The use of nanostructured electrodes, including nanoparticles, have been reported to lower detection limits and increase sensitivity by providing an increased surface area-to-volume ratio for protein immobilization [17].

The selectivity of the sensor was also examined by challenging it with relatively high amounts (10^4–10^5 cfu mL^{-1}) of heat-killed *Staphylococcus aureus* (HKSA) and heat-killed *Salmonella typhimurium* (HKST) as negative controls. Nyquist plots shown in Supplementary Fig. S8 and data presented in Fig. 4 indicate that the *E. coli* biosensor exhibits a negligible response to the negative controls, demonstrating the high selectivity over other bacteria. Incubation of HKEC to PrG-thiol modified gold electrode, in the absence of the IgG, did not result in any appreciable signal (Supplementary Fig. S8), confirming the dose-response curves obtained in Fig. 4b are due to direct receptor-ligand binding rather than generic interaction with the surface.

Conclusions

This report describes the development of a multilayered, self-assembled ultrasensitive impedimetric biosensor for the detection of *E. coli* O157:H7 using gold nanoparticles and thiolated protein G as a foundation for creating a layer of highly oriented antibodies. The work also compares the performances of the gold nanoparticles modified electrode with that of planar gold electrodes. The architecture of the biosensor layers provides ease of fabrication, good EIS performance with affinity to HKEC. The gold nanoparticles-based biosensors detects the bacteria over a broad range of concentrations (>10^5) with a clinically relevant detection limit (48 cfu mL^{-1}). This low limit of detection contrast favorably to the one achieved when using planar gold electrode (140 cfu mL^{-1}) and to most literature reported values for EIS and SPR detection of *E. coli* O157:H7, underlining the importance of gold nanoparticles and oriented antibody immobilization strategy used in this work to enhance the performance of the biosensor. The sensitivity of gold nanoparticles-based biosensor was also superior to that of the planar gold-based biosensor, while the reproducibility of both sensor constructs were excellent. The reproducibility of the sensors' fabrication (relative standard deviation), determined by measuring the charge transfer resistance of the sensor with the IgG layer in buffer, was found to be <1% (n = 5) for both sensor constructs. Negative control experiments using high concentrations of HKSA and HKST exhibited negligible response, demonstrating the high selectivity of the sensors. The combination of self-assembly, high reproducibility, high sensitivity, and regeneration makes the biosensor's design attractive to the development of fast, portable and inexpensive detection platforms.

Acknowledgements The authors acknowledge the support from the NRC-Nanotechnology Research Centre, Defence Research and Development Canada – Suffield Research Centre, and Defence Research and Development Canada Technology Development Fund.

Compliance with ethical standards The author(s) declare that they have no competing interests.

References

1. Majowicz SE, Scallan E, Jones-Bitton A, Sargeant JM, Stapleton J, Angulo FJ, Yeung DH, Kirk MD (2014) Global incidence of human Shiga toxin-producing Escherichia coli infections and deaths: a systematic review and knowledge synthesis. Foodborne Pathog Dis 11:447–455
2. Tokarskyy O, Marshall DL (2008) Immunosensors for rapid detection of Escherichia coli O157:H7 — perspectives for use in the meat processing industry. Food Microbiol 25:1–12
3. Velusamy V, Arshak K, Korostynska O, Oliwa K, Adley C (2010) An overview of foodborne pathogen detection: in the perspective of biosensors. Biotechnol Adv 28:232–254
4. Mayer CL, Leibowitz CS, Kurosawa S, Stearns-Kurosawa DJ (2012) Shiga toxins and the pathophysiology of hemolytic uremic syndrome in humans and animals. Toxins 4:1261–1287
5. Fung F, Wang H-S, Menon S (2018) Food safety in the 21st century. Biom J 41:88–95
6. Varadi L, Luo JL, Hibbs DE, Perry JD, Anderson RJ, Orenga S, Groundwater PW (2017) Methods for the detection and identification of pathogenic bacteria: past, present, and future. Chem Soc Rev 46:4818–4832
7. Amiri M, Bezaatpour M, Jafari H, Boukherroub R, Szunerits S (2018) Electrochemical methodologies for the detection of pathogens. ACS Sensors 3:1069–1086
8. Chen Y, Wang Z, Liu Y, Wang X, Li Y, Ma P, Gu B, Li H (2014) Recent advances in rapid pathogen detection method based on biosensors. Eur J Clin Microbiol Infect Dis 37:1021–1037
9. Yoo SM, Lee SY (2016) Optical biosensors for the detection of pathogenic microorganisms. Trends Biotechnol 34:7–25
10. Dong Z-M, Zhao G-C (2015) Label-free detection of pathogenic bacteria via immobilized antimicrobial peptides. Talanta 137:55–61
11. Xu M, Wang R, Li Y (2017) Electrochemical biosensors for rapid detection of Escherichia coli O157:H7. Talanta 162:511–522
12. Heo J, Hua SZ (2009) An overview of recent strategies in pathogen sensing. Sensors 9:4483–4502
13. Chang B-Y, Park S-M (2010) Electrochemical impedance spectroscopy. Annu Rev Anal Chem 3:207–229
14. Zhu C, Yang G, Li H, Du D, Lin Y (2015) Electrochemical sensors and biosensors based on nanomaterials and nanostructures. Anal Chem 87:230–249

15. Tran TB, Son SJ, Min J (2016) Nanomaterials in label-free impedimetric biosensor: current process and future perspectives. BioChip J 10:318–330
16. Lin D, Harris KD, Chan NWC, Jemere AB (2018) Nanostructured indium tin oxide electrodes immobilized with toll-like receptor proteins for label-free electrochemical detection of pathogen markers. Sensors Actuators B Chem 257:324–330
17. Jans H, Huo Q (2012) Gold nanoparticle-enabled biological and chemical detection and analysis. Chem Soc Rev 41:2849–2866
18. Lin D, Tang T, Harrison DJ, Lee WE, Jemere AB (2015) A regenerating ultrasensitive electrochemical impedance immunosensor for the detection of adenovirus. Biosens Bioelectron 68:129–134
19. Zhang J, Wang J, Zhu J, Xu J, Chen H, Xu D (2008) An electrochemical impedimetric arrayed immunosensor based on indium tin oxide electrodes and silver-enhanced gold nanoparticles. Microchim Acta 163:63–70
20. Zhou J, Du L, Zou L, Zou Y, Hu N, Wang P (2014) An ultrasensitive electrochemical immunosensor for carcinoembryonic antigen detection based on staphylococcal protein A—au nanoparticle modified gold electrode. Sensors Actuators B Chem 197:220–227
21. Wang Y, Ping J, Ye Z, Wu J, Ying Y (2013) Impedimetric immunosensor based on gold nanoparticles modified graphene paper for label-free detection of Escherichia coli O157:H7. Biosens Bioelectron 49:492–498
22. Yang H, Zhou H, Hao H, Gong Q, Nie K (2016) Detection of Escherichia coli with a label-free impedimetric biosensor based on lectin functionalized mixed self-assembled monolayer. Sensors Actuators B Chem 229:297–304
23. Geng P, Zhang X, Meng W, Wang Q, Zhang W, Jin L, Feng Z, Wu Z (2008) Self-assembled monolayers-based immunosensor for detection of Escherichia coli using electrochemical impedance spectroscopy. Electrochim Acta 53:4663–4668
24. Ruan C, Yang L, Li Y (2002) Immunobiosensor chips for detection of Escherichia coli O157:H7 using electrochemical impedance spectroscopy. Anal Chem 74:4814–4820
25. Maalouf R, Fournier-Wirth C, Coste J, Chebib H, Saikali Y, Vittori O, Errachid A, Cloarec J-P, Martelet C, Jaffrezic-Renault N (2007) Label-free detection of bacteria by electrochemical impedance spectroscopy: comparison to surface plasmon resonance. Anal Chem 79:4879–4886
26. dos Santos MB, Agusil JP, Prieto-Simon B, Sporer C, Teixeria V, Samitier J (2013) Highly sensitive detection of pathogen Escherichia coli O157:H7 by electrochemical impedance spectroscopy. Biosens Bioelectron 45:174–180
27. dos Santos MB, Azevedo S, Agusil JP, Prieto-Simon B, Sporer C, Torrents E, Juarez A, Teixeira V, Samitier J (2015) Label-free ITO-based immunosensor for the detection of very low concentrations of pathogenic bacteria. Bioelectrochem 101:146–152
28. Joung C-K, Nim H-N, Lim M-C, Jeon T-J, Kim H-Y, Kim YR (2013) A nanoporous membrane-based impedimetric immunosensor for label-free detection of pathogenic bacteria in whole milk. Biosens Bioelectron 44:210–215
29. Fowler JM, Stuart MC, Wong DKY (2007) Self-assembled layer of thiolated protein G as an Immunosensor scaffold. Anal Chem 79: 350–354
30. Kausaite-Minkstimiene A, Ramanaviciene A, Kirlyte J, Ramanavicius A (2010) Comparative study of random and oriented antibody immobilization techniques on the binding capacity of immunosensor. Anal Chem 82:6401–6408
31. Makaraviciute A, Ramanaviciene A (2013) Site-directed antibody immobilization techniques for immunosensors. Biosens Bioelectron 50:460–471
32. Trilling AK, Beekwilder J, Zuilhof H (2013) Antibody orientation on biosensor surfaces: a minireview. Analyst 138:1619–1627
33. Liu Y, Yu J (2016) Oriented immobilization of proteins on solid supports for use in biosensors and biochips: a review. Microchim Acta 183:1–19
34. Turkova J (1999) Oriented immobilization of biologically active proteins as a tool for revealing protein interactions and function. J Chromatogr B Biomed Sci Appl 722:11–31
35. Hafaiedh I, Chammem H, Abdelghani A, Ait E, Feldman L, Meilhac O, Mora L (2013) Supported protein G on gold electrode: characterization and immunosensor application. Talanta 116:84–90
36. Mahmoud AM, Tang T, Harrison DJ, Lee WE, Jemere AB (2014) A regenerating self-assembled gold nanoparticle-containing electrochemical impedance sensor. Biosens Bioelectron 56:328–333
37. Sun X, Zhu Y, Wang X (2011) Amperometric immunosensor based on a protein A/deposited gold nanocrystals modified electrode for carbofuran detection. Sensors 11:11679–11691
38. Janek RP, Fawcett WR (1998) Impedance spectroscopy of self-assembled monolayers on Au (111): sodium ferrocyanide charge transfer at modified electrode. Langmuir 14:3011–3018
39. Shein JB, Lai LMH, Eggers PK, Paddon-Row MN, Gooding JJ (2009) Formation of efficient electron transfer pathways by adsorbing gold nanoparticles to self-assembled monolayer modified electrodes. Langmuir 25:11121–11128
40. Adams KL, Jena BK, Percival SJ, Zhang B (2011) Highly sensitive detection of exocytotic dopamine release using a gold-nanoparticle-network microelectrode. Anal Chem 83:920–927
41. Bertok T, Sediva A, Vikartovska A, Tkac J (2014) Comparison of the 2D and 3D nanostructured lectin-based biosensors for in situ detection of sialic acid on glycoproteins. Int J Electrochem Sci 9: 890–900
42. Baccar H, Mejri MB, Hafaiedh I, Ktari T, Aouni M, Abdelghani A (2010) Surface plasmon resonance immunosensor for bacteria detection. Talanta 82:810–814